ACS SENSORS

pubs.acs.org/acssensors

Article

Smart Bioelectronic Nanomesh Face Masks with Permeability and Flexibility for Monitoring Cortisol in Saliva

Sungjoon Cho, Chihyeong Won, Chaebeen Kwon, Hwajoong Kim, Sanghyeon Lee, Kukro Yoon, Minkyu Lee, Jinho Kim, Mugeun Lee, Seungmin Lee, Jinhan Lee, Enming Song, Yongfeng Mei, Jaehong Lee,* and Taeyoon Lee*

Cite This: *ACS Sens.* 2025, 10, 148−158

Read Online

ACCESS | Metrics & More | Article Recommendations | Supporting Information

ABSTRACT: Bioelectronic face masks can easily collect biomarkers in saliva, in which free cortisol is abundant. However, conventional bioelectronic face masks involve significant challenges in terms of permeability and inhalation due to their nonpermeable film-type structure. Herein, we introduce a flexible and permeable nanomesh-based wearable biosensor designed for bioelectronic face masks that monitor cortisol levels. The diameter of the nanofiber matrix has a range of 200 to 500 nm and offers outstanding flexibility (2% resistance change at a bending radius of 2 mm), reliability (0.3% resistance change at a bending radius of 5 mm after 1000 bending cycles), and permeability (116.91 g m^{-2} h^{-1} at 18 °C with 40% humidity, which is 10 times higher compared with film) based on the nanoporous structure. We evaluated the electrochemical responses of functionalized interdigitated electrodes on a flexible and permeable poly(vinylidene fluoride-*co*-hexafluoropropylene) (PVDF-HFP) nanomesh. Our nanomesh cortisol biosensors demonstrated exceptional sensitivity to cortisol, even at low concentrations, with a detection limit as low as 10 pM. Furthermore, we measured cortisol in clinical samples, such as artificial saliva and human saliva, using nanomesh-based bioelectronic face masks. This study highlights the potential for further applications of bioelectronic face masks for detecting numerous biomarkers.

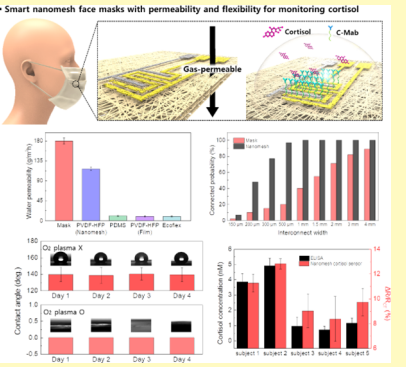

KEYWORDS: *permeable electrodes, wearable biosensors, bioelectronic face masks, nanomesh, saliva detection*

Stress has detrimental effects on both physical and mental health, leading to a variety of health issues, reduced cognitive abilities, strained relationships, and decreased overall quality of life.[1,2] Cortisol, a glucocorticoid hormone, is a well-established biomarker for stress, and it plays significant roles in various physiological functions such as maintaining glucose levels and promoting metabolism in daily life.[3,4] Monitoring cortisol in daily life is crucial for enhancing quality of life, because abnormal cortisol levels may result in obesity, fatigue, and diseases of hormonal imbalance such as Cushing's syndrome and Addison's disease.[5,6]

Traditional methods for measuring cortisol levels have involved the use of enzyme-linked immunosorbent assays (ELISA), liquid chromatography−tandem mass spectrometry (LC−MS/MS), and lateral flow tests, which are limited in terms of complex equipment and restricted testing locations.[7,8] These methods typically require specialized equipment, trained personnel, and specific laboratory settings for quantitative measurements, which can limit their use in daily life.[9−11] Especially, lateral flow tests are fast and have high accuracy, making them convenient to use.[12,13] However, additional equipment is required to assess the signal's color intensity, size, and other parameters for measuring cortisol levels. Furthermore, multiple steps, such as capturing and interpreting optical signals, need to be considered, along with factors like environmental lighting conditions, to ensure sufficient sensitivity and accuracy, which restrict their usability in everyday life. To address these issues, there has been a growing focus on the development of flexible and wearable biosensors that can provide a more accessible and user-friendly approach to cortisol measurement.[14−16]

Recent advances in cortisol monitoring biosensors demonstrate the monitoring of cortisol levels using flexible and wearable bioskin patches to analyze various biofluids such as sweat.[15−18] Demuru et al. fabricated organic electrochemical transistors (OECTs) on flexible polyimide substrates as wearable biosensors that measure cortisol levels in sweat.[16] However, conventional skin-attached biosensors often require additional steps, such as sweat induction through physical activity or chemical iontophoretic (IP) sweat stimulation, and

Received: June 23, 2024
Revised: December 24, 2024
Accepted: December 30, 2024
Published: January 13, 2025

they primarily focus on cortisol measurement, which may limit their versatility and user-friendliness.[19,20] Sweat induction can be inconvenient and can affect the accuracy of measurements, especially because physical activity influences cortisol levels.[2]

Accordingly, there is a demand for wearable devices that utilize alternative biofluids such as saliva.[2,21,22] Bioelectronic face masks, being in close contact with the respiratory system, can conveniently collect oral fluids naturally produced during routine actions such as coughing and speaking, while also performing the function of a mask.[23,24] Furthermore, the demand for mask-type wearable devices has been increasing in everyday life due to factors such as fine dust and respiratory diseases.[25,26] Wang et al. fabricated ion-gated transistors (IGTs) integrated with breath valves in wearable bioelectronic face masks.[27] Integrated IGTs enabled the bioelectronic face mask to detect various respiratory infectious diseases without inducing oral fluids. Nguyen et al. fabricated lateral flow assay (LFA) indicator strips integrated into face masks that could detect bacterial nucleic acids noninvasively.[28] However, previous research also indicated that bioelectronic face masks lacked gas permeability due to their rigid substrate, leading to reduced comfort in practical use.[29] Furthermore, there have been no studies on bioelectronic face masks that measure the cortisol levels of oral fluids such as saliva, and it is important to note that cortisol is not present in exhaled breath. The cortisol in saliva exists completely in its free form, as bound cortisol is effectively removed due to the filtration process in the salivary glands.[14,30] In cases where a person has pneumonia or adrenal disorders, their bound cortisol levels significantly decrease or fluctuate, which makes it challenging to accurately measure the total cortisol quantity.[31] Hence, it has become crucial to measure the free cortisol in saliva instead.

In this study, we present an approach for developing smart bioelectronic nanomesh face masks that enable the monitoring of the cortisol levels in a user's saliva with flexibility and permeability. Typically, the materials of face masks are constructed as a mesh to allow for gas permeability while enhancing particulate capture efficiency.[32,33] Nanomesh also possesses gas permeability, and due to its high efficiency in particulate capture, it is a viable material for face mask fabrication.[34] Our nanomesh biosensors showed great permeability and flexibility, which allowed for seamless integration with the face masks.[29,34−37] Moreover, our nanomesh cortisol biosensors demonstrated remarkable sensitivity to cortisol in a low range of concentrations with a detection limit as low as 10 pM. These findings verify the suitability of our biosensors for accurately measuring cortisol levels in human saliva samples. Finally, our nanomesh cortisol biosensors integrated into the commercial face masks were used to determine cortisol levels in artificial and human saliva, compared with ELISA. These results significantly expand the potential applications of mask-type wearable cortisol biosensors and showcase their versatility and promising utility.

EXPERIMENTAL SECTION

Materials. Poly(vinylidene fluoride-*co*-hexafluoropropylene) (PVDF-HFP), *N*,*N*-dimethylformamide (DMF), sodium borohydride ($NaBH_4$), hydrogen chloride (HCl), dichloromethane (DCM), ethanolamine (EA), phosphate-buffered saline (PBS), potassium ferricyanide(III) ($K_3Fe(CN)_6$), and artificial saliva were obtained from Sigma-Aldrich. For evaluating the selectivity of cortisol biosensors, cortisol, corticosterone, cortisone, glucose, urea, and lactic acid were obtained from Sigma-Aldrich. For functionalization of the electrode, dithiobis(succinimidyl propionate) (DTSP) and cortisol monoclonal antibody (C-Mab) were purchased from Thermo Fisher Scientific. Commercial yellow dust prevention masks, which can filter fine particles of 0.4 μm average size at over 94%, were obtained from Tamsa.

Device Fabrication. The PVDF-HFP solution (24 wt %) was prepared by mixing PVDF-HFP pellets with DCM, followed by stirring at 80 °C for 2 h. The PVDF-HFP nanomesh was prepared by electrospinning. The nanofiber was electrospun for 2 h at room temperature. Aluminum foil was placed on the collector to collect PVDF-HFP nanofibers. The applied voltage was 20 kV, the flow rate was 0.3 mL h^{-1}, and the distance between the nozzle (23 G needle) and the collector was 15 cm. Interdigitated electrodes were fabricated on the nanomesh by using thermal evaporation. After the Au and Ag patterns (120 nm of thickness) were deposited using a shadow mask, Ag was chlorinated by electroplating. The electrodes are immersed in HCl solution (0.1 M) for 10 min, applying a DC power supply (0.6 V) to electroplate Ag.[38,39] Then, the electrodes were cleaned by using DI water. Before functionalization, the electrode was plasma treated at 100 W for 60 s to change the wettability of surfaces (CUTE-MPR, Femto Science) using a shadow mask.[40,41] The wettability of the treated area changed from hydrophobic to hydrophilic. After oxygen plasma treatment, an additional PVDF-HFP solution is electrospun onto sensors directly to insulate interconnects over 2 h. A thickness of over 300 μm for the insulating layer can facilitate the repeatability and reproducibility of the sensor. If the immersion time in PBS solution or saliva exceeds 10 min, they can penetrate the insulating nanomesh, given that the nanomesh is sufficiently thin.

Fabrication. The electrode was immersed in a DTSP/DCM solution for 2 h (8 mg mL^{-1}).[42] The DTSP was reduced by using sodium borohydride (10 mg mL^{-1} in DI water). After the electrodes were cleaned using DI water to remove any unbound DTSP, the electrodes were dried in a refrigerator at 4 °C for 12 h or overnight.[43] Next, a C-Mab solution (10 μL) was immobilized on the electrodes for 2 h (10 mM in PBS, pH 7.4). The succinimidyl group of the DTSP/Au electrode binds to the amino group of C-Mab. To block the unreacted succinimidyl group of the DTSP, EA (10 μL) was immobilized on the electrodes for 5 min. After the electrodes were cleaned using DI water, the functionalized electrodes were stored in a refrigerator at 4 °C when not in use.

Water Vapor Permeation Experiments. Water vapor permeability was evaluated by measuring the loss of water by weight in an opened poly bottle.[29] The opening of the bottle was covered with the nanomesh and reference samples. A sample, both having a diameter of 35 mm, was filled with 2 g of DI water. An adhesive (Araldite, Nichiban) was used to attach a nanomesh sheet to the bottle's opening. The bottle was then placed in a thermostatic chamber set to 18 °C with 40% humidity for 3 days, and the subsequent decrease in weight was recorded. As reference samples, PVDF-HFP film (10 μm thickness), aluminum foil (1 μm thickness), polydimethylsiloxane (PDMS) (10 μm thickness), and ecoflex film (10 μm thickness) were utilized.

Mask Inhalation Resistance Measurement. Upon affixing, the test specimen was affixed to the face region of the test mannequin to ensure no deformation and prevent any air leakage. The pressure differential (Pa) was determined when the air was made to traverse continuously at a flow rate of 30 L per minute. The mask inhalation resistance measurement was evaluated by measuring the pressure differential of the air leakage. The mask inhalation resistance of the commercial face mask, the PVDF-HFP nanomesh-covered face mask, and the PVDF-HFP film-covered face mask was assessed. The nanomesh and the film (10 μm thickness each) were affixed to the face masks using adhesive tape (n = 3).

Electrochemical Responses for Saliva Measurement through the Bioelectronic Face Masks. The potential application of nanomesh cortisol biosensors was demonstrated by the introduction of commercial yellow dust prevention masks integrated with nanomesh cortisol biosensors (Figure S1). The mannequins wore bioelectronic face masks, which measured the electrochemical responses. The airbrush was connected with an air pressure regulator to disperse the spread of artificial saliva or human saliva onto the

https://doi.org/10.1021/acssensors.4c01531
ACS Sens. 2025, 10, 148−158

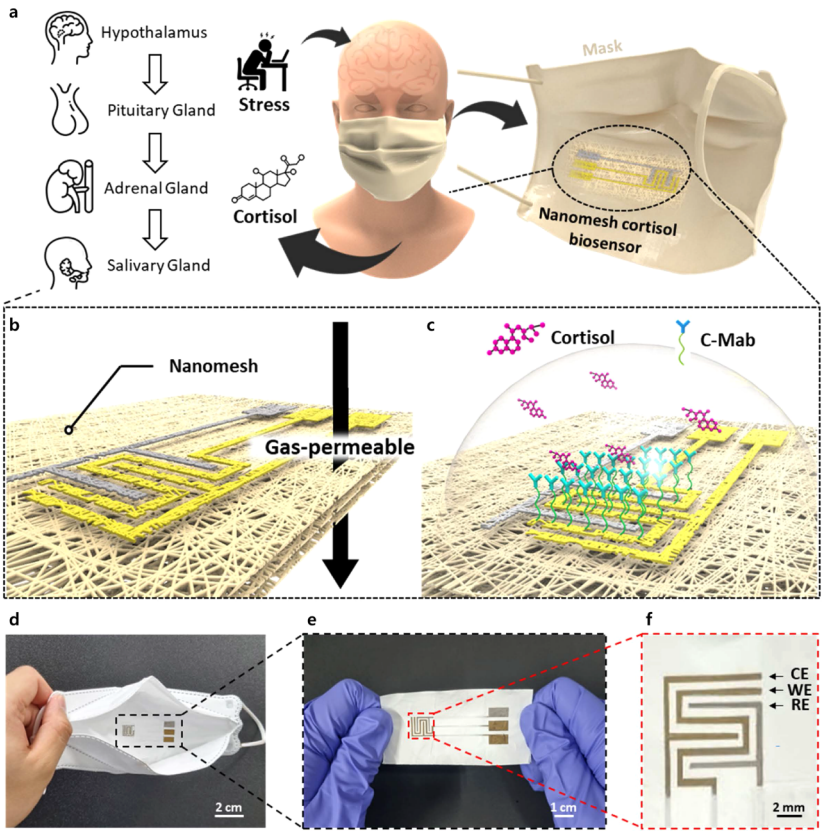

Figure 1. (a) Overall schematic of nanomesh cortisol biosensor in the bioelectronic face mask. Cortisol levels are controlled by the hypothalamus-pituitary-adrenal axis. (b) Schematic of the gas permeable nanomesh-based biosensor. The gas permeable property results from the porous structure of the nanomesh. (c) Schematic of the nanomesh-based cortisol biosensor for measuring the cortisol in saliva. (d) Nanomesh cortisol biosensor embedded in the bioelectronic face mask. (e) Bioelectrodes on the flexible nanomesh. (f) Interdigitated structure of working electrode (WE), counter electrode (CE), and reference electrode (RE) on the nanomesh.

bioelectronic masks. The applied air pressure was 20 kPa, which was the same as the average air pressure of a mild cough.[44] The nozzle with a 0.3-mm diameter was used in our experimental setup, as it aligns with the naturally occurring droplet size range of 0.1−0.3 mm.[45−47] The artificial saliva and human saliva were tested to evaluate bioelectronic face masks. The saliva was dispersed using an airbrush that mimicked the pressure equivalent to a mild cough. Artificial saliva (Fusayama/Meyer), where cortisol (from 100 pM to 100 nM) was added, was used. Human saliva samples were collected at 9 a.m. from a volunteer in a fasting state after they had first rinsed their mouth with water for 30 s. The saliva samples were stored at −20 °C before use. Before the electrochemical responses of human saliva were measured, 0.1 mL of PBS was spread on the surface of bioelectronic face masks to measure the initial electrochemical responses. The volunteers involved in collecting saliva are also the coauthors of this manuscript. No ethical approval was required in this case.

Characterization. Field emission scanning electron microscopy (FE-SEM; JSM-IT500HR) was used to obtain mesh structure images of the nanomesh sensors and face masks. The nanomesh diameter and pore area distribution of the nanomesh sensors and face masks were analyzed by using JSM-IT500HR FE-SEM and ImageJ software. A cyclic bending test was carried out using a motorized X-translation stage (Jaeil Optical Corp., Korea). The electrical characteristics were measured using a 2450 sourcemeter (Kiethly, USA). A potentiostat (SP-200, Bio-Logic, USA) was used to conduct cyclic voltammetry (CV), square wave voltammetry (SWV), and electrochemical impedance spectroscopy (EIS). The Fourier-transform infrared (FTIR) spectrum of the sensors was obtained by using a spectrometer (Vertex 70, Bruker). The X-ray photoelectron spectroscopy (XPS) spectrum of the electrodes was obtained using a Thermo Fisher Scientific K-alpha. To evaluate the cortisol concentrations in the saliva, the ELISA (Cortisol ELISA kit, ENZO) test was carried out. The optical density of the ELISA plate was obtained by using a multilabel plate reader (Victor 5).

RESULTS AND DISCUSSION

Design and Fabrication of Smart Bioelectronic Nanomesh Face Mask. The cortisol levels in the human body are regulated by the hypothalamus-pituitary-adrenal (HPA) axis in response to stress, leading to the diffusion of cortisol from the bloodstream to the salivary glands (Figure 1a). We developed smart bioelectronic nanomesh face masks that are permeable and flexible and that monitor cortisol levels in saliva. As illustrated in Figure 1b,c, the bioelectronic face mask was designed to maintain the characteristics of gas permeability and flexibility without compromising the face mask's functionality and to provide an electrochemical sensing capacity to the face mask. A nanomesh exhibits superior permeability compared to film, as it retains nanosized pores for the passage of gas (Figure 1b). Similarly, metal patterns are evaporated onto the nanomesh that exhibited high permeability due to its nanosized pores. After the self-assembled monolayer (SAM)-modified electrodes were functionalized, the electrochemical properties were characterized by using EIS and CV (Figure 1c). The charge transfer resistance and oxidation current peak were measured to evaluate the hindrance of electron movement from binding of cortisol and C-Mab.

https://doi.org/10.1021/acssensors.4c01531
ACS Sens. 2025, 10, 148−158

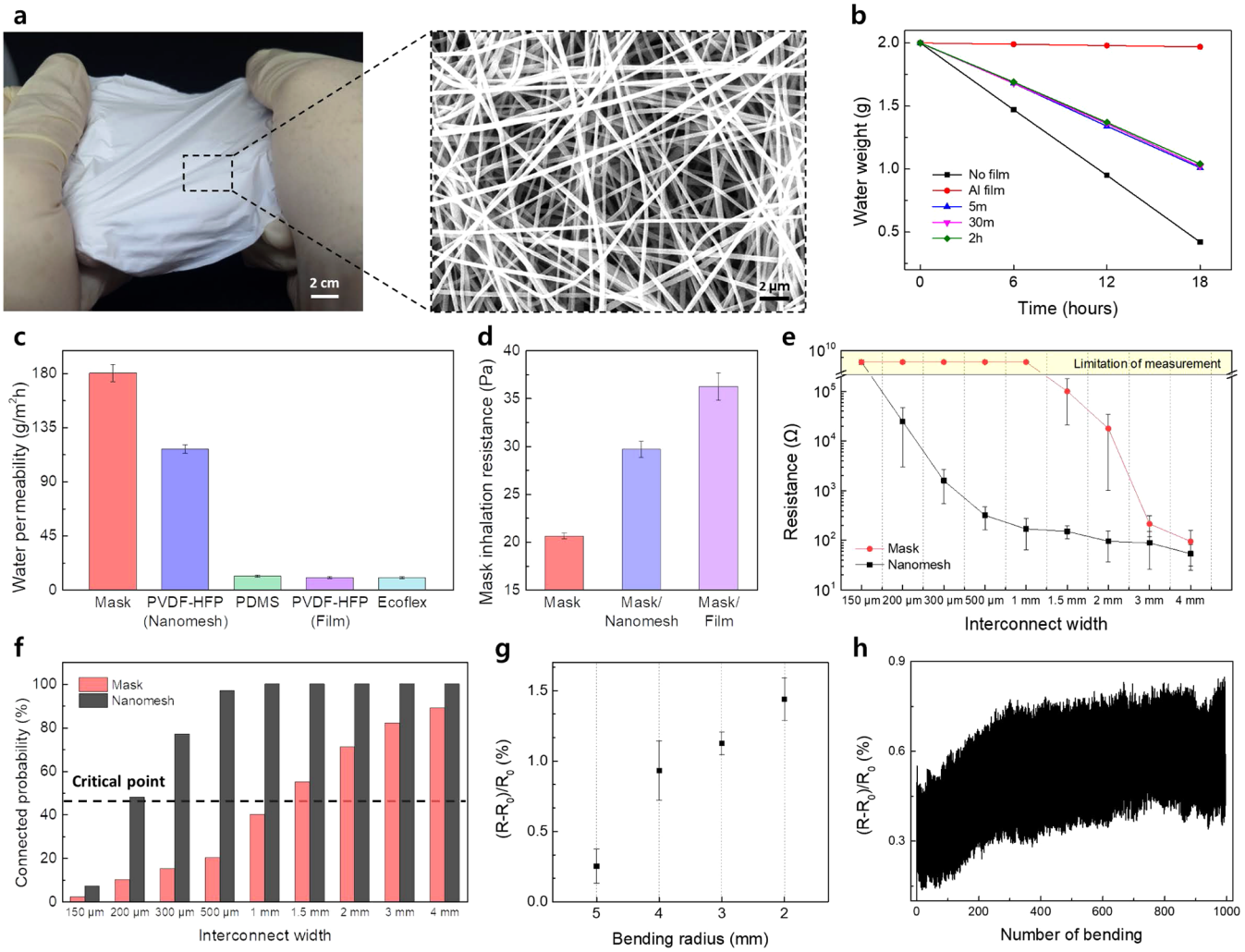

Figure 2. (a) Optical and SEM images of the flexible PVDF-HFP nanomesh. (b) Water vapor permeability test for the nanomesh fabricated with different electrospinning times, the aluminum film, and the control group. (c) Water vapor permeability for different materials. (d) Mask inhalation resistance of commercial face masks, PVDF-HFP nanomesh-covered face masks, and PVDF-HFP film-covered face masks. (e) Resistance of interconnect for the commercial face mask and PVDF-HFP nanomesh (n = 4) according to the width of interconnect. (f) Connected probability simulation for different interconnect widths of the simulated mask and nanomesh. For each interconnect width, 100 simulation repetitions were conducted. (g) Resistive change in nanomesh with bending radii of 5, 4, 3, and 2 mm (n = 4). (h) Repetitive bending test with a bending radius of 5 mm over 1000 cycles.

Figure 1d depicts the developed bioelectronics face mask integrated with nanomesh-based cortisol biosensors, which possess gas-permeable characteristics and are capable of measuring the electrochemical response of biosensors to cortisol in saliva. A nanomesh is formed by electrospinning a PVDF-HFP solution, which has high chemical resistance and mechanical strength, onto a commercial face mask and depositing electrodes by using a thermal evaporator (Figure 1d). After the electrodes are patterned, an additional PVDF-HFP solution is electrospun onto the sensors directly to insulate the interconnect (Figure 1e). The detailed fabrication process is shown in Figure S2. After the nanomesh is fabricated, the SAM-modified interdigitated electrodes were functionalized to measure the electrochemical response of the cortisol biosensors to the cortisol in saliva. Figure 1f presents three digitated electrodes, which were designed to increase the surface area of the adjacent electrodes.[48] Each electrode had a width and thickness of 500 μm and 120 nm, respectively. For reference electrodes, silver electrodes were chlorinated by electroplating to the Ag-deposited electrodes. The XPS spectra of the Ag 3d and Cl 2p regions revealed that the electrodes contain Ag and Cl atoms (Figure S3).[38,49]

Characterization of Nanomesh. Given that the control of the viscoelastic properties of the polymer is of paramount importance to the electrospinning process, parameters such as flow rate, concentration, and applied voltage were determined to be the key factors in optimizing the formation of the nanomesh (Figures S4 and S5).[50] As shown in Figure 2a, the nanomesh under investigation exhibited flexibility with an average nanofiber diameter of 250 nm (Figure S6). As evidenced by the SEM images, the nanomesh structure, which was composed of numerous nanofibers, formed a multitude of nanoscale pores (Figure 2a). These nanoscale pores, formed by overlapping nanofibers, exhibited superior permeability compared with conventional film structures. We validated this by utilizing the water vapor permeation method to evaluate how the permeability varies with the electrospinning time to optimize the thickness of the nanomesh (Figures 2b and S7). The water vapor permeability of our nanomesh was 116.91 g m^{-2} h^{-1}, which was slightly lower

https://doi.org/10.1021/acssensors.4c01531
ACS Sens. 2025, 10, 148−158

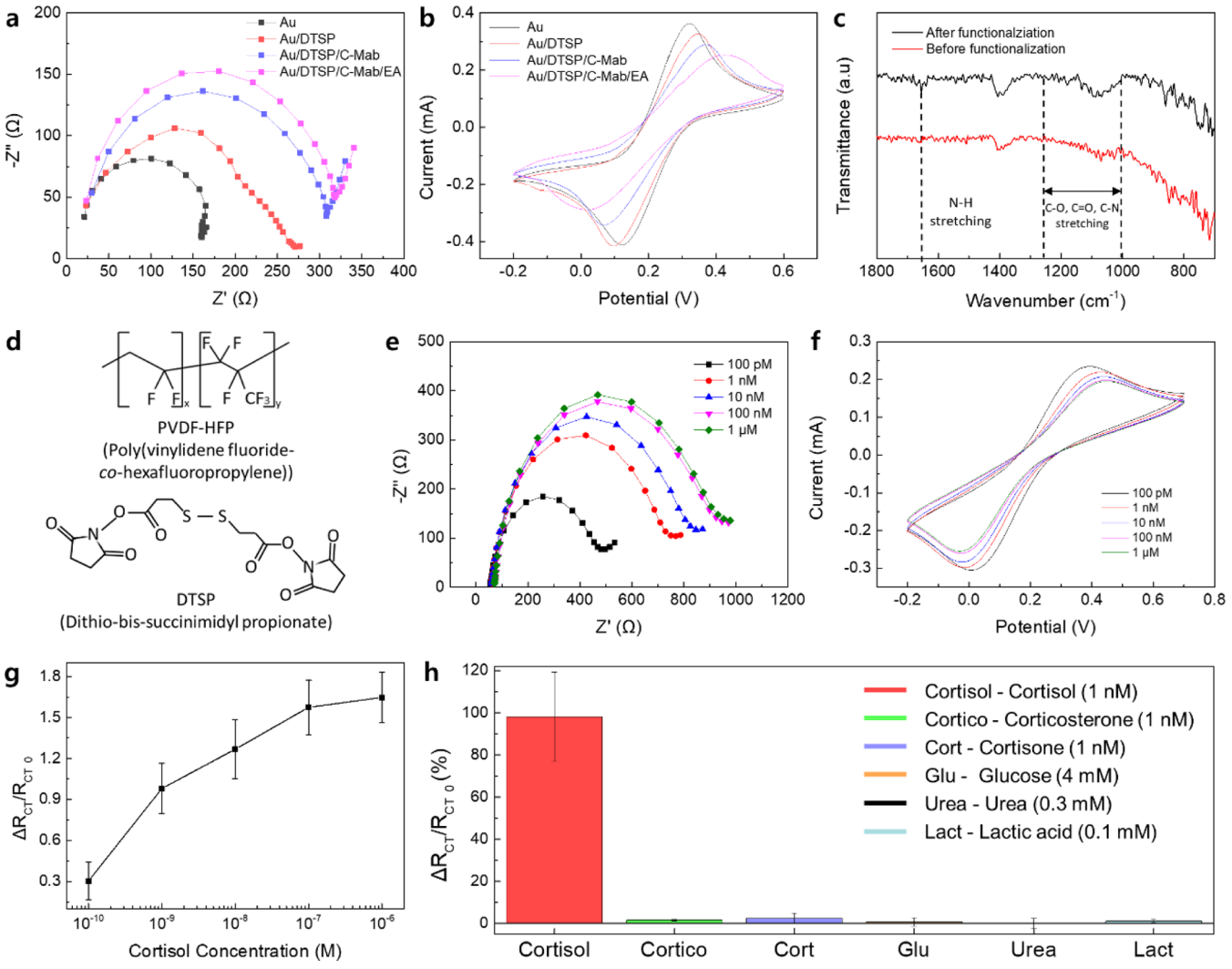

Figure 3. (a) Nyquist plots of Au, Au/DTSP, Au/DTSP/C-Mab, and AU/DTSP/C-Mab/EA bioeletrodes. (b) CV curves for Au, Au/DTSP, Au/DTSP/C-Mab, and AU/DTSP/C-Mab/EA bioeletrodes. (c) FTIR spectroscopy of Au electrodes before functionalization (red) and after functionalization (black). (d) Molecular structures of PVDF-HFP and DTSP. (e) Nyquist plots of the nanomesh cortisol biosensors for different concentrations of cortisol from 100 pM to 1 μM. (f) CV curve of the nanomesh cortisol biosensors for different cortisol concentrations from 100 pM to 1 μM. (g) Electrochemical response of the nanomesh cortisol biosensors to cortisol concentration (from 100 pM to 1 μM, n = 3) and calibration curve (R^2 = 0.88). (h) Electrochemical response to cortisol, other steroid hormones, and substances (n = 3).

compared to the face mask and opened poly bottle (180.12 g m^{-2} h^{-1}, 193.63 g m^{-2} h^{-1} each) (Figure 2c). The water vapor permeabilities of PDMS, PVDF-HFP film, and ecoflex were 10.96 g m^{-2} h^{-1}, 9.74 g m^{-2} h^{-1}, and 9.74 g m^{-2} h^{-1} each (Figure 2c).

This demonstrates that the nanomesh structure possesses a water vapor permeability that is at least 10-fold superior to that of conventional polymer films. Furthermore, this trend was also discernible in the measurements of mask inhalation resistance (Figure 2d). Mask inhalation resistance refers to the degree of breathing difficulty attributable to the face mask when worn on the face. To demonstrate that the nanomesh had lower mask inhalation resistance than the film, the mask inhalation resistances of a pristine face mask, nanomesh-covered face mask, and film-covered face mask were evaluated. The mask inhalation resistances were found to be 20.58, 29.65, and 36.24 Pa for the pristine face mask, nanomesh-covered face mask, and film-covered face mask, respectively (Figure 2d). The nanomesh-covered face mask exhibited a higher mask inhalation resistance compared to a film-covered face mask, making it easier to breathe through.

Figure 2e illustrates the resistance of the interconnect relative to the width of the metal pattern interconnect in both the nanomesh and micromesh structures of the face mask for an interconnect length of 30 mm. The resistance of the interconnect was rapidly increased with increased interconnect width. Furthermore, interconnects with a nanomesh structure exhibited superior conductivity compared to those with a micromesh structure of the face masks. This performance can be attributed to the connectivity, which refers to the extent of being interconnected between fibers of the conductive mesh structure. Interconnects were not established at lower interconnect widths (under 150 μm) of nanomesh and micromesh of face masks, which can be attributed to falling below the minimum connectivity of a conductive mesh network required for interconnects (Figures 2e and S8). However, as the diameter of the fibers decreases, the number of interconnected fibers per unit width increases, which may increase the connectivity. The increased connectivity led to an

https://doi.org/10.1021/acssensors.4c01531
ACS Sens. 2025, 10, 148−158

increase in the number of conductive paths, which in turn resulted in a marked decrease in resistance. Consequently, metal patterns of nanomesh structure have superior conductivity compared to a micromesh structure of face masks.

The connectivity of the interconnects was simulated by measuring the probability of connecting randomly generated lines using a Python code (Figure S9). Initially, the number of randomly generated lines was set by comparing the simulated average pore area with the average pore area of a commercial face mask and a PVDF-HFP nanomesh. The commercial face mask's average pore area was 3085.927 μm^2 (Figure S10). In contrast, the average pore areas derived from randomly generated lines were 3,417 μm^2, 1,843 μm^2, and 1234 μm^2 for N = 100, 200, and 300, respectively (Figure S11). Consequently, the number of generated lines simulating the face masks was fixed at 100 based on the closest resemblance to the face mask's average pore area (Figure S11). Likewise, the number of generated lines simulating the nanomesh was determined as 20,000 by comparing the average simulated pore areas with the average actual pore areas. After these lines were generated, intersections among all of the lines were identified. In the final step, these intersections were categorized under "interconnect" and were visually represented with appropriate color coding (Figures S12 and S13). During the simulation, it was observed that the connected probability, which refers to the probability of forming an interconnect in several simulations, sharply decreased as the width of the interconnect decreased, validating the increased resistance as the width of the interconnect decreased (Figure 2f). The connected probability of the nanomesh decreased at a lower interconnect width compared to the face mask, indicating the superior connectivity of the nanomesh compared to the face mask. The greater number of randomly generated lines and the greater number of interconnected fibers per unit width resulted in the superior connectivity of the nanomesh. When the simulated connected probability was compared with the actual resistance for different interconnect widths, neither the nanomesh nor the face mask established connections when the probability was below a critical point of 45%.

To demonstrate that the electrical properties of the nanomesh remained when the nanomesh was bent and stretched, bending and stretching tests were conducted. Even at a bending radius of 2 mm, where the bending radius refers to the curvature of the nanomesh, the electrode exhibited a rate of change in resistance of less than 2% (Figure 2g). Furthermore, to assess its durability, the bending test was repeated 1000 times at a bending radius of 5 mm (Figure 2h). Upon the conclusion of the repeated tests, while there was a slight increase in the resistance, the resistance was recovered to 0.3% of the original level. Also, the electrode exhibited a rate of change in resistance of less than 60% at a strain of 5% (Figure S14). After 1000 times of stretching test, the resistance was recovered to 3% of the original level.

Electrochemical Sensing Performance. The electrochemical characteristics of the progressively constructed biosensor electrode were examined by using EIS (Figure 3a). EIS characterization was carried out in PBS (pH 7.4) containing 5 mM $[Fe(CN)^6]^{3-}$ over a frequency range from 100 kHz to 0.5 Hz. The charge transfer resistance, which is characterized by the radius of the semicircle in the Nyquist plot, was found to increase after the deposition of the DTSP (Figure 3a). This suggests that when the DTSP forms on the electrode, it creates an insulating layer and a physical barrier. This insulating layer and physical barrier impede electrical connection and hinder electron movement, leading to an increase in charge transfer resistance.[43] After the sequential immobilization of C-Mab and EA, the charge transfer resistance was found to increase due to the hindered movement of electrons. The immobilization of EA occupies the unoccupied sites between C-Mab and DTSP, leading to an increase in the charge transfer resistance. Furthermore, the step-by-step assembly of the biosensor electrode was analyzed using CV to evaluate the electrochemical properties (Figure 3b). CV characterization was carried out in PBS (pH 7.4) containing 5 mM $[Fe(CN)^6]^{3-}$ at a scan rate of 20 mV s^{-1}. A pair of redox peaks were observed, indicating that well-defined oxidation and reduction occurred. The electrochemical current, which encompassed both the oxidation current peak and reduction current peak, sequentially decreased with the deposition of DTSP and the immobilization of C-Mab and EA. As previously mentioned, this decrease can be attributed to the hindrance of electron movement caused by each material.

The FTIR spectra of the DTSP-deposited electrodes were measured before and after the deposition of the SAM to further identify the functionalization (Figure 3c,d). As depicted in Figure 3d, unlike DTSP, the PVDF-HFP material lacks amine groups, carboxyl groups, C−O, and C−N bonds, which is evident from its FTIR transmission spectra.[51] A C−F peak of PVDF-HFP can be discerned in the range of 1400−1300 cm^{-1}, irrespective of functionalization. For the functionalized sample, a newly emergent N−H peak can be detected in the range of 1650−1580 cm^{-1}, and there is a notable increase in transmission attributable to C═O, C−O, and C−N bonding within the 1000−1260 cm^{-1} range.

The electrochemical response was examined using EIS, CV, and SWV in response to different cortisol concentrations in the PBS solution under identical characterization conditions (Figures 3e,f and S15). The incubation time was set to the duration at which no further change in the electrochemical response could be observed, which was typically established to be 30 min. Electrochemical measurements were conducted by adding cortisol solutions every 30 min while keeping the sample immobile. The cortisol solutions were prediluted in PBS to achieve the target concentrations, ranging from 100 pM to 1 μM. Each prediluted cortisol solution was introduced step by step to monitor the changes in the electrochemical response. As the concentration of cortisol increased, the charge transfer resistance was observed to increase correspondingly, with an estimated detection limit of 10 pM and a correlation coefficient of 0.88 (Figure 3e,g). This resulted from binding between C-Mab and cortisol, leading to increased hindrance in electron movement. Furthermore, the oxidation and reduction current peaks in the CV curve decreased linearly as the concentration of cortisol increased from 100 pM to 1 μM (Figure 3f).

The selectivity of the cortisol biosensor was demonstrated by measuring other steroid hormones and substances (corticosterone, cortisone, glucose, uric acid, and lactic acid). To validate its selectivity, all substances were tested at their estimated physiological concentrations, and the cortisol biosensor exhibited negligible responses to other substances compared with cortisol (Figure 3h). Also, we conducted in vitro experiments using a PBS solution containing mucin (1.19 mg/mL) to ensure that the signal is specific. As a control sensor, we used an IL-6 sensor, which is an antibody-labeled sensor designed to capture the release of IL-6 during immune

https://doi.org/10.1021/acssensors.4c01531
ACS Sens. 2025, 10, 148−158

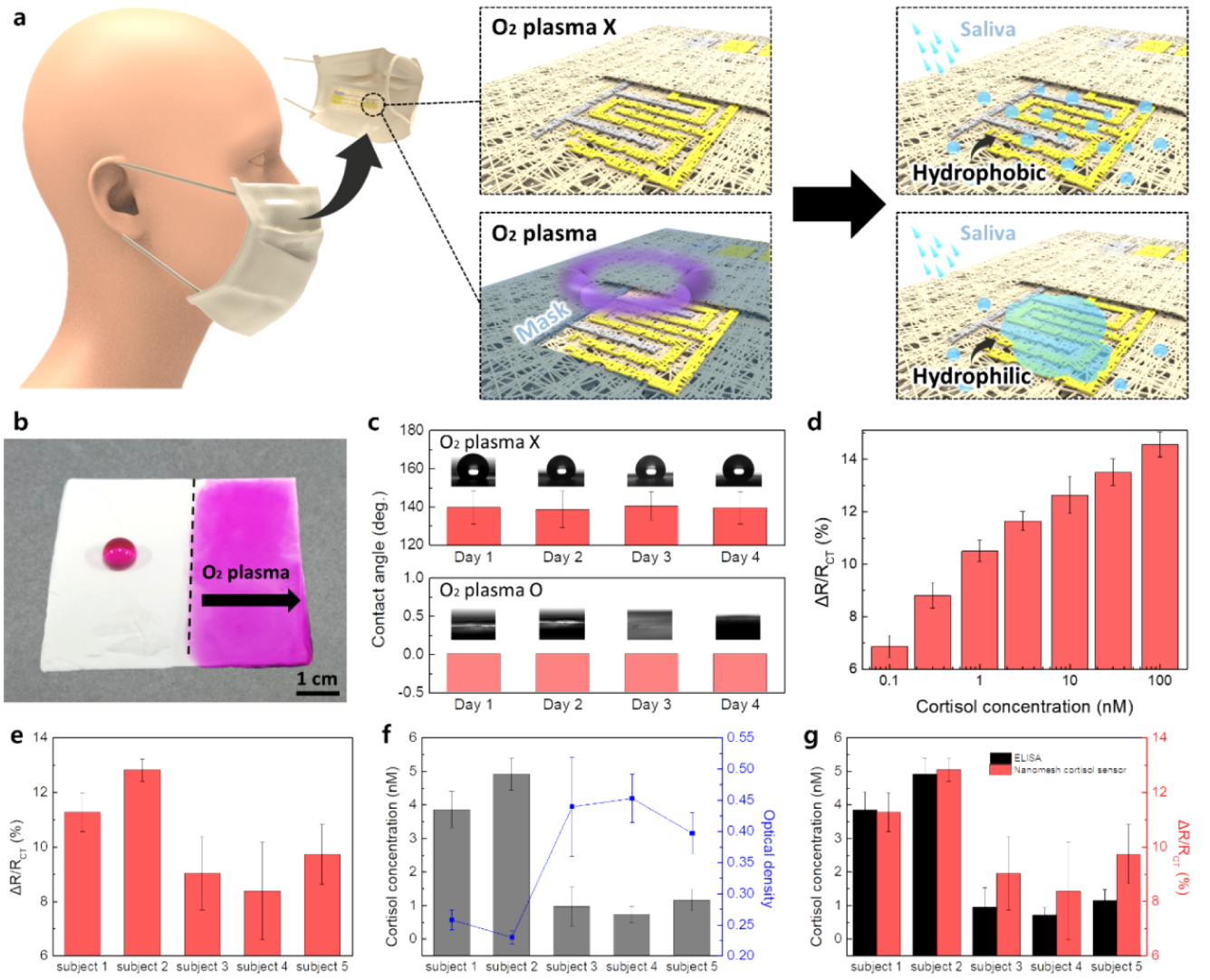

Figure 4. (a) Schematic of wettability of nanomesh surface after oxygen plasma treatment. (b) Comparison between wettabilities of the nanomesh surface before and after oxygen plasma treatment. DI water containing rhodamine B was spread on the surface. (c) Contact angle of nanomesh according to the duration of oxygen plasma treatment (n = 3). (d) Change in charge transfer resistance for different cortisol concentrations in artificial saliva (0.1, 0.3, 1, 3, 10, 30, and 100 nM) (n = 3). (e) Charge transfer resistance change for the subject's actual saliva samples (n = 3). (f) ELISA results, cortisol concentration, and optical density of the subject's actual saliva samples (n = 3). (g) Comparison of ELISA and nanomesh cortisol biosensors.

responses. For the cortisol sensor, we observed a noticeable increase in charge transfer resistance (R_{ct}), consistent with the presence of cortisol in the saliva sample. In contrast, the IL-6 sensor, which is designed to detect the IL-6 protein, exhibited a significantly lower R_{ct} compared with the cortisol sensor. This experiment confirmed the specificity of the sensors, with the cortisol sensor specifically detecting cortisol.

Also, changes in charge transfer resistance were observed with different concentrations of steroid hormones to demonstrate that the electrochemical signals of the sensors were specific to cortisol concentrations (Figure S16). When exposed to the other substances tested, the signal changes were less than 5%, indicating that these changes were not significant compared with signal changes to cortisol. This signifies that the sensor did not respond to other substances such as corticosterone, cortisone, glucose, uric acid, and lactic acid.

Measurement of Cortisol in Clinical Samples Using the Smart Bioelectronic Face Mask. Figure 4a illustrates the fabrication process used to enhance the wettability of the sensor surface for application in face masks. Although the hydrophobic nature of the nanomesh may help droplets of saliva flow through the surface of a face mask, the electrodes in the biosensor did not connect through saliva, as the saliva droplets were not evenly spread. Accordingly, surface treatment was required to collect saliva onto the electrodes. Oxygen plasma treatment was utilized as the surface treatment to increase the surface energy of the electrode surface without damaging the nanomesh structure. Before the functionalization, the wettability of the electrodes was converted to hydrophilic by an oxygen plasma treatment with a shadow mask. Figure 4b illustrates the wettability of the nanomesh with a shadow mask covering half of the nanomesh before and after the oxygen plasma treatment. The dispensed droplets consist of a PBS solution containing pink dye. The surface exposed to the oxygen plasma exhibits hydrophilic characteristics. To verify the enhancement of wettability by oxygen plasma treatment, the contact angle was measured (Figure 4c). Before the oxygen plasma treatment, the average contact angle was

https://doi.org/10.1021/acssensors.4c01531
ACS Sens. 2025, 10, 148−158

141°, indicating a highly hydrophobic surface. After the oxygen plasma treatment, the surface was observed to be completely wet, leading to the absence of a discernible contact angle. Furthermore, the wettability of the surface was verified to evaluate the stability of the improved wettability over 14 days, revealing no significant deviations (Figure S17). The sensors were continuously stored in a fume hood to maintain a consistent and controlled atmosphere, minimizing potential external factors that could affect their lifespan. The droplets were no longer absorbed into the nanomesh within 10 s, and the contact angle increased after 16 days of storage (Figure S17). Through scanning electron microscopy (SEM) imaging, the potential damage to the mesh structure postplasma treatment was assessed, and it was concluded that the mesh configuration had remained intact (Figure S18).

The electrochemical responses of the bioelectronic face masks were evaluated by using different cortisol concentrations, ranging from 100 pM to 100 nM, in the artificial saliva (Figure 4d). The artificial saliva solution, which contains different cortisol concentrations, was sprayed using an airbrush at 30-min intervals of the incubation period to observe the electrochemical responses. The bioelectronic face mask requires a 30-min incubation period for cortisol detection, which is comparable to traditional saliva collection methods, such as spitting. However, the mask collects saliva over time without the need for user intervention, offering a more practical and unobtrusive solution for monitoring cortisol levels. In addition, the mask continues to serve its primary function as a protective mask, ensuring user convenience and comfort while also facilitating hormone monitoring. The linear responses for the change in charge transfer resistance were investigated. Also, we evaluated whether conventional breathing could affect the R_{CT} of cortisol sensors. To investigate the effect of conventional breathing on the R_{CT}, we conducted experiments using a mannequin equipped with our mask sensor (Figure S19). We utilized PBS solution as a baseline control and PBS solution with mucin (1.19 mg/mL) during these tests to simulate the composition and viscosity of saliva and evaluate the impact of mucin on the sensor's signal. The breathing effect was simulated by supplying air through a hose in intervals of 1 s every 5 s to mimic the exhalation (0.3 kPa).[52] We measured the charge transfer resistance at various time intervals (30 min, 1, 2, 3, and 4 h). The results indicated that when PBS solution was supplied during the measurements, the charge transfer resistance exhibited less than 10% of variation over time (Figure S19). As mucin gradually adhered to the electrode surface, we observed a consistent increase in R_{CT} over time. When conducting experiments with increasing concentrations of cortisol, the presence of mucin led to baseline R_{CT} values that were higher than those of the control group without mucin. By analyzing the relationship between R_{CT} and mucin concentration, we were able to calibrate the sensor's electrical characteristics in response to varying cortisol levels. Importantly, we observed similar response trends in cortisol concentration when mucin was absent, confirming that the sensor retained its performance even without mucin. Additionally, to assess the impact of saliva presence, we measured the charge transfer resistance both with and without the continuous supply of a PBS solution. PBS and PBS with mucin were sprayed using the same pressure and intervals as those of the air supply. The results indicated that when PBS solution was supplied during the measurements, the charge transfer resistance exhibited minimal variation over time (less than 5%), which is not significant enough to affect cortisol measurements. However, when PBS solution was not supplied, a substantial increase in R_{CT} was observed. As the liquid evaporated, there was eventually no electrolyte left to maintain the electrical connection, increasing the impedance until measurements were no longer possible.

The electrochemical responses of the face masks were evaluated in the subject's saliva (Figure 4e). The R_{CT} change of cortisol sensors was measured to estimate the cortisol levels of the five subjects. Following measuring the initial R_{CT} of cortisol sensors, the subject's saliva was sprayed using an airbrush, and the electrochemical measurements were taken after a 30-min incubation period to measure the changes of R_{CT}. ELISA was performed to compare the electrochemical responses by nanomesh cortisol biosensors for analyzing the concentration of cortisol in the subject's saliva (Figure 4f). The cortisol concentration was calculated by using the standard curve from the optical density of the ELISA (Figure S20). A comparison with the electrochemical responses of nanomesh cortisol biosensors and cortisol concentration from the ELISA is shown in Figure 4g. Also, we investigated potential skin irritation issues of the nanomesh-based cortisol biosensors, which are critical for its practical applications. For ensuring the biosensor's safety and comfort for long-term wear, the skin irritation test was conducted for the PVDF-HFP nanomesh and PVDF-HFP films to compare the breathability. Medical tape was used to fix the patches (3M). The nanomesh and film were detached from the right forearm after 4 days. No skin irritations were observed after detaching the nanomesh, whereas the PVDF-HFP film caused red spots on the skin (Figure S21). The results of this comparison suggest that our nanomesh cortisol biosensors can be used as potential bioelectronic face masks, possessing permeability and flexibility.

CONCLUSIONS

In conclusion, we have developed a nanomesh-based, permeable, and flexible cortisol biosensor that can be integrated into bioelectronic face masks. Our flexible nanomesh-based substrates exhibited superior water vapor permeability and mask inhalation resistance relative to film-based substrates, and this makes them suitable for use as substrates for bioelectronic face masks. Furthermore, the dense arrangement of the nanomesh-based substrates resulted in higher connectivity and enhanced conductivity and stability as an interconnect. The nanomesh cortisol biosensors showed excellent sensitivity (with a detection limit of 10 pM), linearity ($R^2 \sim 0.88$), and selectivity. Our bioelectronic face masks integrated with nanomesh cortisol biosensors was successfully shown to easily collect saliva and measure electrochemical responses to human saliva. This study demonstrated that the biomarker in human saliva could be measured using simple bioelectronic face masks. Moreover, this study extended the boundary of application for simply measuring biomarkers in human saliva. However, it is important to note that our current setup involves directly connecting the electrodes to an electrochemical station. Future work should focus on integrating a wireless transmission module and electrochemical system, which would enable the seamless communication of signals between the user and the monitoring device. Given the remarkable performance of our nanomesh cortisol biosensors, we anticipate future innovations for detecting various

https://doi.org/10.1021/acssensors.4c01531
ACS Sens. 2025, 10, 148−158

biomarkers, creating gas-permeable devices, and developing wearable bioelectronics.

■ ASSOCIATED CONTENT

Supporting Information

The Supporting Information is available free of charge at https://pubs.acs.org/doi/10.1021/acssensors.4c01531.

The face model with the nanomesh cortisol biosensor in the bioelectric mask; fabrication process of hydrophilic electrodes on the nanomesh; XPS analysis of the Ag/AgCl electrode and Ag electrode; SEM images of the PVDF-HFP nanofibers in different weight percent; SEM images of the PVDF-HFP nanofibers in different flow rate; diameter distribution of PVDF-HFP nanomesh; water vapor permeability test; schematic diagram of the reduced interconnect connectivity; schematic diagram of simulation of the interconnect connectivity; SEM image of nanomesh and face masks; average pore area of commercial face mask; the randomly generated lines of the width; repetitive stretching test; SWV curve of the nanomesh cortisol biosensors; electrochemical response to cortisol and other steroid hormones; comparison between wettabilities of nanomesh surface and surfaces; SEM image of the PVDF-HFP nanomesh after oxygen plasma treatment; comparison of R_{CT} with the electrochemical responses with additional PBS and without additional PBS; standard curves of ELISA for optical density; skin irritation test (PDF).

■ AUTHOR INFORMATION

Corresponding Authors

Taeyoon Lee − *School of Electrical and Electronic Engineering, Yonsei University, Seoul 03722, Republic of Korea;* orcid.org/0000-0002-8269-0257; Phone: 82-2-2123-7454; Email: taeyoon.lee@yonsei.ac.kr

Jaehong Lee − *Department of Robotics and Mechatronics Engineering, Daegu Gyeongbuk Institute of Science and Technology, Daegu 42988, Republic of Korea;* orcid.org/0000-0002-8779-5293; Phone: 82-53-785-6228; Email: jaelee@dgist.ac.kr

Authors

Sungjoon Cho − *School of Electrical and Electronic Engineering, Yonsei University, Seoul 03722, Republic of Korea*

Chihyeong Won − *School of Electrical and Electronic Engineering, Yonsei University, Seoul 03722, Republic of Korea; Andrew and Peggy Cherng Department of Medical Engineering, Division of Engineering and Applied Science, California Institute of Technology, Pasadena, California 91125, United States*

Chaebeen Kwon − *School of Electrical and Electronic Engineering, Yonsei University, Seoul 03722, Republic of Korea*

Hwajoong Kim − *Department of Robotics and Mechatronics Engineering, Daegu Gyeongbuk Institute of Science and Technology, Daegu 42988, Republic of Korea*

Sanghyeon Lee − *School of Electrical and Electronic Engineering, Yonsei University, Seoul 03722, Republic of Korea*

Kukro Yoon − *School of Electrical and Electronic Engineering, Yonsei University, Seoul 03722, Republic of Korea*

Minkyu Lee − *School of Electrical and Electronic Engineering, Yonsei University, Seoul 03722, Republic of Korea*

Jinho Kim − *Department of Robotics and Mechatronics Engineering, Daegu Gyeongbuk Institute of Science and Technology, Daegu 42988, Republic of Korea*

Mugeun Lee − *Department of Robotics and Mechatronics Engineering, Daegu Gyeongbuk Institute of Science and Technology, Daegu 42988, Republic of Korea*

Seungmin Lee − *School of Electrical and Electronic Engineering, Yonsei University, Seoul 03722, Republic of Korea*

Jinhan Lee − *School of Electrical and Electronic Engineering, Yonsei University, Seoul 03722, Republic of Korea*

Enming Song − *Department of Materials Science, Fudan University, Shanghai 200433, China*

Yongfeng Mei − *Department of Materials Science, Fudan University, Shanghai 200433, China;* orcid.org/0000-0002-3314-6108

Complete contact information is available at: https://pubs.acs.org/10.1021/acssensors.4c01531

Notes

The authors declare no competing financial interest.

■ ACKNOWLEDGMENTS

This research was supported by the National R&D Program through the National Research Foundation of Korea (NRF) funded by the Ministry of Science and ICT (RS-2023-00234581, RS-2021-NR061513). This research was encouraged by the International Joint Research Grant by Yonsei Graduate School.

■ REFERENCES

(1) Burke, H. M.; Davis, M. C.; Otte, C.; Mohr, D. C. Depression and Cortisol Responses to Psychological Stress: A Meta-Analysis. *Psychoneuroendocrinology* **2005**, *30* (9), 846−856.

(2) Ku, M.; Kim, J.; Won, J. E.; Kang, W.; Park, Y. G.; Park, J.; Lee, J. H.; Cheon, J.; Lee, H. H.; Park, J. U. Smart, Soft Contact Lens for Wireless Immunosensing of Cortisol. *Sci. Adv* **2020**, *6* (28), No. eabb2891.

(3) Putman, P.; Antypa, N.; Crysovergi, P.; Van Der Does, W. A. J. Exogenous Cortisol Acutely Influences Motivated Decision Making in Healthy Young Men. *Psychopharmacology* **2010**, *208* (2), 257−263.

(4) Barcellos, L. J. G.; Volpato, G. L.; Barreto, R. E.; Coldebella, I.; Ferreira, D. Chemical Communication of Handling Stress in Fish. *Physiol. Behav* **2011**, *103* (3−4), 372−375.

(5) Widmer, I. E.; Puder, J. J.; König, C.; Pargger, H.; Zerkowski, H. R.; Girard, J.; Müller, B. Cortisol Response in Relation to the Severity of Stress and Illness. *J. Clin. Endocrinol. Metab* **2005**, *90* (8), 4579−4586.

(6) Filaire, E.; Rouveix, M.; Alix, D.; Le Scanff, C. M. Motivation, Stress, Anxiety, and Cortisol Responses in Elite Paragliders. *Percept. Mot. Skills* **2007**, *104* (3_suppl), 1271−1281.

(7) Pearlmutter, P.; DeRose, G.; Samson, C.; Linehan, N.; Cen, Y.; Begdache, L.; Won, D.; Koh, A. Sweat and Saliva Cortisol Response to Stress and Nutrition Factors. *Sci. Rep* **2020**, *10* (1), 19050.

(8) Jo, S.; Lee, W.; Park, J.; Kim, W.; Kim, W.; Lee, G.; Lee, H. J.; Hong, J.; Park, J. Localized Surface Plasmon Resonance Aptasensor for the Highly Sensitive Direct Detection of Cortisol in Human Saliva. *Sens. Actuators, B* **2020**, *304* (August 2019), 127424.

(9) Lee, H.-B.; Meeseepong, M.; Trung, T. Q.; Kim, B. Y.; Lee, N. E. A Wearable Lab-on-a-Patch Platform with Stretchable Nanostructured Biosensor for Non-Invasive Immunodetection of Biomarker in Sweat. *Biosens. Bioelectron* **2020**, *156* (December 2019), 112133.

(10) Yoon, S. S.; Lee, K. E.; Cha, H. J.; Seong, D. G.; Um, M. K.; Byun, J. H.; Oh, Y.; Oh, J. H.; Lee, W.; Lee, J. U. Highly Conductive Graphene/Ag Hybrid Fibers for Flexible Fiber-Type Transistors. *Sci. Rep* **2015**, *5*, 16366.
(11) Santiago-Malagón, S.; Río-Colín, D.; Azizkhani, H.; Aller-Pellitero, M.; Guirado, G.; Del Campo, F. J. A Self-Powered Skin-Patch Electrochromic Biosensor. *Biosens. Bioelectron* **2021**, *175* (October2020), 112879.
(12) Oh, H. K.; Kim, J. W.; Kim, J. M.; Kim, M. G. High Sensitive and Broad-Range Detection of Cortisol in Human Saliva Using a Trap Lateral Flow Immunoassay (TrapLFI) Sensor. *Analyst* **2018**, *143* (16), 3883−3889.
(13) Dalirirad, S.; Han, D.; Steckl, A. J. Aptamer-Based Lateral Flow Biosensor for Rapid Detection of Salivary Cortisol. *ACS Omega* **2020**, *5* (51), 32890−32898.
(14) Ok, J.; Sumin Park, S.; Jung, Y. H.; Kim, T.-I. Wearable and Implantable Cortisol-Sensing Electronics for Stress Monitoring. *Adv. Mater* **2024**, *36* (1), 2211595.
(15) Wang, B.; Zhao, C.; Wang, Z.; Yang, K.; Cheng, X.; Liu, W.; Yu, W.; Lin, S.; Zhao, Y.; Cheung, K. M.; Lin, H.; Hojaiji, H.; Weiss, P. S.; Stojanović, M. N.; Tomiyama, A. J. Wearable Aptamer-Field-Effect Transistor Sensing System for Noninvasive Cortisol Monitoring. *Sci. Adv* **2022**, *8* (1), No. eabk0967.
(16) Demuru, S.; Kim, J.; El Chazli, M.; Bruce, S.; Dupertuis, M.; Binz, P. A.; Saubade, M.; Lafaye, C.; Briand, D. Antibody-Coated Wearable Organic Electrochemical Transistors for Cortisol Detection in Human Sweat. *ACS Sens* **2022**, *7* (9), 2721−2731.
(17) An, J. E.; Kim, K. H.; Park, S. J.; Seo, S. E.; Kim, J.; Ha, S.; Bae, J.; Kwon, O. S. Wearable Cortisol Aptasensor for Simple and Rapid Real-Time Monitoring. *ACS Sens* **2022**, *7*, 99.
(18) Parlak, O.; Keene, S. T.; Marais, A.; Curto, V. F.; Salleo, A. Molecularly Selective Nanoporous Membrane-Based Wearable Organic Electrochemical Device for Noninvasive Cortisol Sensing. *Sci. Adv* **2018**, *4* (7), No. eaar2904.
(19) Xu, Z.; Qiao, X.; Tao, R.; Li, Y.; Zhao, S.; Cai, Y.; Luo, X. A Wearable Sensor Based on Multifunctional Conductive Hydrogel for Simultaneous Accurate PH and Tyrosine Monitoring in Sweat. *Biosens. Bioelectron* **2023**, *234* (April), 115360.
(20) Kim, J.; Sempionatto, J. R.; Imani, S.; Hartel, M. C.; Barfidokht, A.; Tang, G.; Campbell, A. S.; Mercier, P. P.; Wang, J. Simultaneous Monitoring of Sweat and Interstitial Fluid Using a Single Wearable Biosensor Platform. *Adv. Sci* **2018**, *5* (10), 1800880.
(21) Stevens, R. C.; Soelberg, S. D.; Near, S.; Furlong, C. E. Detection of Cortisol in Saliva with a Flow-Filtered, Portable Surface Plasmon Resonance Biosensor System. *Anal. Chem* **2008**, *80* (17), 6747−6751.
(22) Tlili, C.; Myung, N. V.; Shetty, V.; Mulchandani, A. L.-F. Label-free, chemiresistor immunosensor for stress biomarker cortisol in saliva. *Biosens. Bioelectron* **2011**, *26* (11), 4382−4386.
(23) Maier, D.; Laubender, E.; Basavanna, A.; Schumann, S.; Güder, F.; Urban, G. A.; Dincer, C. Toward Continuous Monitoring of Breath Biochemistry: A Paper-Based Wearable Sensor for Real-Time Hydrogen Peroxide Measurement in Simulated Breath. *ACS Sens* **2019**, *4* (11), 2945−2951.
(24) Daniels, J.; Wadekar, S.; DeCubellis, K.; Jackson, G. W.; Chiu, A. S.; Pagneux, Q.; Saada, H.; Engelmann, I.; Ogiez, J.; Loze-Warot, D.; Boukherroub, R.; Szunerits, S. A Mask-Based Diagnostic Platform for Point-of-Care Screening of Covid-19. *Biosens. Bioelectron* **2021**, *192* (July), 113486.
(25) Kim, J. H.; Marcus, C.; Ono, R.; Sadat, D.; Mirzazadeh, A.; Jens, M.; Fernandez, S.; Zheng, S.; Durak, T.; Dagdeviren, C. A Conformable Sensory Face Mask for Decoding Biological and Environmental Signals. *Nat. Electron* **2022**, *5*, 794.
(26) Escobedo, P.; Fernández-Ramos, M. D.; López-Ruiz, N.; Moyano-Rodríguez, O.; Martínez-Olmos, A.; Pérez de Vargas-Sansalvador, I. M.; Carvajal, M. A.; Capitán-Vallvey, L. F.; Palma, A. J. Smart Facemask for Wireless CO2Monitoring. *Nat. Commun* **2022**, *13* (1), 72.
(27) Wang, B.; Yang, D.; Chang, Z.; Zhang, R.; Dai, J.; Fang, Y. Wearable Bioelectronic Masks for Wireless Detection of Respiratory Infectious Diseases by Gaseous Media. *Matter* **2022**, *5* (12), 4347−4362.
(28) Nguyen, P. Q.; Soenksen, L. R.; Donghia, N. M.; Angenent-Mari, N. M.; de Puig, H.; Huang, A.; Lee, R.; Slomovic, S.; Galbersanini, T.; Lansberry, G.; Sallum, H. M.; Zhao, E. M.; Niemi, J. B.; Collins, J. J. Wearable Materials with Embedded Synthetic Biology Sensors for Biomolecule Detection. *Nat. Biotechnol* **2021**, *39* (11), 1366−1374.
(29) Nayeem, M. O. G.; Lee, S.; Jin, H.; Matsuhisa, N.; Jinno, H.; Miyamoto, A.; Yokota, T.; Someya, T. A. N. B. All-nanofiber−based, ultrasensitive, gas-permeable mechanoacoustic sensors for continuous long-term heart monitoring. *Proc. Natl. Acad. Sci. U.S.A* **2020**, *117* (13), 7063−7070.
(30) Inder, W. J.; Dimeski, G.; Russell, A. Measurement of Salivary Cortisol in 2012 - Laboratory Techniques and Clinical Indications. *Clin. Endocrinol* **2012**, *77* (5), 645−651.
(31) Choi, M. H. Clinical and Technical Aspects in Free Cortisol Measurement. *Endocrinol. Metab* **2022**, *37* (4), 599−607.
(32) Lee, J.; Bae, J.; Youn, D. Y.; Ahn, J.; Hwang, W. T.; Bae, H.; Bae, P. K.; Kim, I. D. Violacein-Embedded Nanofiber Filters with Antiviral and Antibacterial Activities. *Chem. Eng. J* **2022**, *444* (April), 136460.
(33) Karim, N.; Afroj, S.; Lloyd, K.; Oaten, L. C.; Andreeva, D. V.; Carr, C.; Farmery, A. D.; Kim, I. D.; Novoselov, K. S. Sustainable Personal Protective Clothing for Healthcare Applications: A Review. *ACS Nano* **2020**, *14* (10), 12313−12340.
(34) Miyamoto, A.; Lee, S.; Cooray, N. F.; Lee, S.; Mori, M.; Matsuhisa, N.; Jin, H.; Yoda, L.; Yokota, T.; Itoh, A.; Sekino, M.; Kawasaki, H.; Ebihara, T.; Amagai, M.; Someya, T. Inflammation-Free, Gas-Permeable, Lightweight, Stretchable on-Skin Electronics with Nanomeshes. *Nat. Nanotechnol* **2017**, *12* (9), 907−913.
(35) Tang, W.; Fu, C.; Xia, L.; Lyu, P.; Li, L.; Fu, Z.; Pan, H.; Zhang, C.; Xu, W. A Flexible and Sensitive Strain Sensor with Three-Dimensional Reticular Structure Using Biomass Juncus Effusus for Monitoring Human Motions. *Chem. Eng. J* **2022**, *438* (March), 135600.
(36) Zhu, D.; Zhang, Z.; Chen, M.; Li, P.; Xiang, Y.; Ouyang, J.; Huang, Z.; Liu, X.; Wang, F.; Yang, M.; Zeng, H.; Hong, P.; Wei, L.; Hou, C.; Tao, G. A Perspective on Rhythmic Gymnastics Performance Analysis Powered by Intelligent Fabric. *Adv. Fiber Mater* **2023**, *5* (1), 1−11.
(37) Yu, Y.; Wang, J.; Han, X.; Yang, S.; An, G.; Lu, C. Fiber-Shaped Soft Actuators: Fabrication, Actuation Mechanism and Application. *Adv. Fiber Mater* **2023**, *5* (3), 868−895.
(38) Wang, P.; Huang, B.; Lou, Z.; Zhang, X.; Qin, X.; Dai, Y.; Zheng, Z.; Wang, X. Synthesis of Highly Efficient Ag@AgCl Plasmonic Photocatalysts with Various Structures. *Chem. -Eur. J* **2010**, *16* (2), 538−544.
(39) de la Rica, R.; Fernández-Sánchez, C.; Baldi, A. Polysilicon Interdigitated Electrodes as Impedimetric Sensors. *Electrochem. Commun* **2006**, *8* (8), 1239−1244.
(40) Bao, B.; Ji, B.; Wang, M.; Gao, K.; Yang, B.; Chen, X.; Wang, X.; Liu, J. Development and Characterisation of Electroplating Silver/Silver Chloride Modified Microelectrode Arrays. *Micro Nano Lett* **2019**, *14* (3), 299−303.
(41) Teo, W. E.; Ramakrishna, S. A Review on Electrospinning Design and Nanofibre Assemblies. *Nanotechnology* **2006**, *17* (14), R89−R106.
(42) Vasudev, A.; Kaushik, A.; Tomizawa, Y.; Norena, N.; Bhansali, S. An LTCC-Based Microfluidic System for Label-Free, Electrochemical Detection of Cortisol. *Sens. Actuators, B* **2013**, *182*, 139−146.
(43) Pandey, P.; Arya, S. K.; Matharu, Z.; Singh, P.; Datta, M.; Malhotra, B. D. Polythiophene Gold Nanoparticles Composite Film for Application to Glucose Sensor. *J. Appl. Polym. Sci* **2008**, *110* (2), 988−994.

https://doi.org/10.1021/acssensors.4c01531
ACS Sens. 2025, 10, 148−158

(44) Baraket, A.; Lee, M.; Zine, N.; Sigaud, M.; Yaakoubi, N.; Trivella, M. G.; Zabala, M.; Bausells, J.; Jaffrezic-Renault, N.; Errachid, A. Diazonium Modified Gold Microelectrodes onto Polyimide Substrates for Impedimetric Cytokine Detection with an Integrated Ag/AgCl Reference Electrode. *Sens. Actuators, B* **2013**, *189*, 165−172.
(45) Schijven, J.; Vermeulen, L. C.; Swart, A.; Meijer, A.; Duizer, E.; de Roda Husman, A. M. Quantitative Microbial Risk Assessment for Airborne Transmission of Sars-Cov-2 via Breathing, Speaking, Singing, Coughing, and Sneezing. *Environ. Health Perspect* **2021**, *129* (4), 1−10.
(46) Xie, X.; Li, Y.; Sun, H.; Liu, L. Exhaled Droplets Due to Talking and Coughing. *J. R. Soc., Interface* **2009**, *6* (SUPPL. suppl_6), S703−S714.
(47) Han, Z. Y.; Weng, W. G.; Huang, Q. Y. Characterizations of Particle Size Distribution of the Droplets Exhaled by Sneeze. *J. R. Soc., Interface* **2013**, *10* (88), 20130560.
(48) Han, H.; Lee, J. S.; Kim, H.; Shin, S.; Lee, J.; Kim, J.; Hou, X.; Cho, S. W.; Seo, J.; Lee, T. Single-Droplet Multiplex Bioassay on a Robust and Stretchable Extreme Wetting Substrate through Vacuum-Based Droplet Manipulation. *ACS Nano* **2018**, *12* (2), 932−941.
(49) Sahoo, B. N.; Woo, J.; Algadi, H.; Lee, J.; Lee, T. S. Superhydrophobic, Transparent, and Stretchable 3D Hierarchical Wrinkled Film-Based Sensors for Wearable Applications. *Adv. Mater. Technol* **2019**, *4* (10), 1900230.
(50) Toma, K.; Oishi, K.; Yoshimura, N.; Arakawa, T.; Yatsuda, H.; Mitsubayashi, K. Repeated Immunosensing by a Dithiobis-(Succinimidyl Propionate)-Modified SAW Device. *Talanta* **2019**, *203* (April), 274−279.
(51) Lee, K. K.; Davenport, P. W.; Smith, J. A.; Irwin, R. S.; McGarvey, L.; Mazzone, S. B.; Birring, S. S.; Abu Dabrh, A. M.; Altman, K. W.; Barker, A. F.; Birring, S. S.; Blackhall, F.; Bolser, C.; Brightling, C.; Chang, A. B.; Davenport, P.; El Solh, A. A.; Escalante, P.; Field, S. K.; Fisher, D.; French, C.; Grant, C.; Harding, S. M.; Harnden, A. T.; Hill, A.; Irwin, R. S.; Iyer, V.; Kahrilas, P. J.; Kavanagh, J.; Keogh, K. A.; Lai, K.; Lane, A.; Lim, K.; Madison, J. M.; Malesker, M.; McGarvey, L.; Murad, M. H.; Narasimhan, M.; Newcombe, P.; Oppenheimer, J. H.; Rubin, B.; Russell, R. J.; Ryu, J. H.; Singh, S. Global Physiology and Pathophysiology of Cough: Part 1: Cough Phenomenology − CHEST Guideline and Expert Panel Report. *Chest* **2021**, *159* (1), 282−293.
(52) Pleil, J. D.; Ariel Geer Wallace, M.; Davis, M. D.; Matty, C. M. The Physics of Human Breathing: Flow, Timing, Volume, and Pressure Parameters for Normal, on-Demand, and Ventilator Respiration. *J. Breath Res* **2021**, *15* (4), 042002.

https://doi.org/10.1021/acssensors.4c01531
ACS Sens. 2025, 10, 148−158